ELSEVIER

Biochimica et Biophysica Acta 1511 (2001) 99–112

BIOCHIMICA ET BIOPHYSICA ACTA
BBA

www.bba-direct.com

Secondary structure in lung surfactant SP-B peptides: IR and CD studies of bulk and monolayer phases

Darline Dieudonné, Richard Mendelsohn, Ramy S. Farid, Carol R. Flach *

Rutgers University, Department of Chemistry, 73 Warren Street, Newark, NJ 07102, USA

Received 20 September 2000; received in revised form 12 December 2000; accepted 14 December 2000

Abstract

Pulmonary surfactant protein SP-B is known to facilitate adsorption and spreading of surfactant components across the air/water interface. This property appears essential for in vivo function in the alveolar subphase and at the air/alveolar surface. Three peptides with amino acid sequences based on SP-B containing predicted α-helical regions (SP-B_{1-20}, SP-B_{9-36A}, SP-B_{40-60A}) have been synthesized to probe structure-function relationships and protein-lipid interaction in bulk phase and monolayer environments. IR and CD studies are reported along with traditional surface pressure-molecular area (π-A) isotherms and IR reflection-absorption spectroscopy (IRRAS) investigations conducted at the air/water interface. In bulk phase, helix-promoting environments (methanol and aqueous dispersions of lipid vesicles), SP-B_{1-20} and SP-B_{9-36A} contained significant amounts of α-helical structure, whereas varying degrees of α-helix, random coil, and β-sheet were observed in aqueous solutions and monolayers. The most striking behavior was observed for SP-B_{9-36A}, which displayed reversible surface pressure-induced β-sheet formation. Bulk phase lipid melting curves and monolayer experiments with peptide-lipid mixtures showed subtle differences in the degree of bulk phase interaction and substantial differences in peptide surface activity. The uniqueness of IRRAS is emphasized as the importance of evaluating secondary structure in both bulk phase and monolayer environments for lung surfactant peptide mimics is demonstrated.

Keywords: Infrared reflection-absorption spectroscopy; Pulmonary surfactant; Surfactant protein B; Lipid-peptide interaction; Langmuir film; Air/water interface

1. Introduction

Biological interfaces impart specific properties to their constituent molecules such as increasing their concentration and orienting them in a specific fashion. A prime example of an interface controlling a key process is the air/alveolar lining of the lung in which pulmonary surfactant functions to facilitate respiration. Pulmonary surfactant is a lipid/protein complex assembled from components (lamellar bodies, tubular myelin, and vesicles) located within the alveolar subphase [1]. As the surface active constituents of surfactant organize at the air/alveolar interface, a monomolecular film (monolayer) is thought to form. The surfactant monolayer allows for the integrity of the alveolar surface to be maintained by withstanding surface tension values near zero upon expiration and aiding in the rapid spread-

* Corresponding author. Fax: +1-973-353-1264;
E-mail: flach@andromeda.rutgers.edu

0005-2736/01/$ – see front matter
PII: S0005-2736(00)00387-4

ing of constituents across the interface during inhalation.

Pulmonary surfactant is composed of approx. 90 weight% lipid and 10% protein. The main lipid component is 1,2-dipalmitoylphosphatidylcholine (DPPC) along with high percentages of unsaturated phosphatidylcholine (PC) and phosphatidylglycerol (PG). Four surfactant-specific proteins have been isolated. Surfactant protein (SP)-B and SP-C are hydrophobic, low molecular weight proteins known to facilitate adsorption and spreading at the air/water (A/W) interface. SP-A and SP-D are multimeric, hydrophilic, collagenous proteins with the ability to bind lipids and are thought to play a role in host-defense activities. In addition, the presence of SP-A and SP-B have been reported as necessary for the formation of tubular myelin, a complex of bilayer structures from which the surface active monolayer is presumed to form. The composition of pulmonary surfactant, its morphology and organization have been reviewed recently [1–3].

Animal-derived surfactant preparations are currently used therapeutically for treating respiratory distress syndrome. Supplementation of exogenous surfactant with specific lipids and/or the hydrophobic proteins, SP-B and SP-C, is also under evaluation although a coherent molecular level understanding of protein function and lipid/protein interaction in lung surfactant does not exist [4,5]. Investigations utilizing a wide variety of biophysical techniques have thus been performed in an attempt to elucidate structure-function relationships of the surfactant proteins, particularly SP-B. The generally accepted structure of SP-B is based on both experiments and homology modeling [2,6]. SP-B is isolated as a disulfide-linked homodimer with each 79 amino acid monomer containing three intramolecular disulfide bonds. Human SP-B carries a net charge of +7. Circular dichroism (CD) and Fourier transform infrared (FTIR) spectroscopic studies of SP-B in organic solutions, lipid micelles, and bilayers report that the protein possesses substantial α-helical content (40–60%) with varying amounts of random coil, β-sheet, and β-turn structure [7–10].

SP-B is known to function in a lipid environment. Experimental methods used to examine SP-B/lipid interaction in membrane models include fluorescence [11,12], differential scanning calorimetry [13], attenuated total reflection (ATR) FTIR [7], Raman spectroscopy [14], deuterium NMR [9,15], and electron spin resonance [12,16]. Different modes of interaction have been described, but the majority of experiments support a peripheral association between SP-B and model membranes varying in the degree of protein penetration into the lipid acyl chain region. In addition, the method of vesicle reconstitution was demonstrated to influence the depth of penetration [12,17].

Peptide analogues of SP-B are currently being evaluated for both therapeutic use and in attempts to elucidate structure-function relationships in the native protein ([5] and references therein; [18,19]). The choice of specific peptide sequences is based on model amphipathic helical motifs and/or the native amino acid sequence. Many of the peptides are evaluated and compared to native SP-B with respect to their conformation in various bulk phase environments and their surface activity in monolayers. However, the secondary structure determined in bulk phase environments may differ from that found in monolayers [20], invalidating the correlations drawn between bulk phase structure and surface activity. It is evident that the determination of the secondary structure of surfactant proteins and related peptides in monolayers is essential for understanding their in vivo function.

To date, only a few studies have attempted to determine the conformation of SP-B in monolayers. In one report, CD spectra were acquired from monolayers transferred to quartz plates (Langmuir-Blodgett films) and an α-helical structure was observed for SP-B both in the presence and absence of lipids [21]. The technique of infrared reflection-absorption spectroscopy (IRRAS) has allowed the acquisition of protein spectra in situ at the A/W interface [22]. In particular, IRRAS has been applied to investigate the surface active properties and secondary structure of SP-B in lipid monolayers [23]. In these studies a mixed helical/random coil structure was reported over a surface pressure range of 20–60 mN/m.

More recent developments in IRRAS have allowed the determination of the orientation of ordered regions within lipid and protein molecules at the A/W interface [24,25]. This determination requires a well defined molecular axis for a particular conformation. For SP-B, the presence of more than one conforma-

tion and in particular, the presence of random coil structure, confounds the orientation measurements. Therefore, in the current study the following approach was adopted: three peptides derived from SP-B and predicted by standard algorithms to contain substantial α-helical content were synthesized to determine their secondary structure in the presence and absence of lipids under conditions of varying surface pressure at the A/W interface with a view to determining their orientation in subsequent studies. The results are compared to bulk phase measurements and traditional surface pressure-molecular area (π-A) isotherms to provide a structural characterization of the peptides and information about peptide/lipid interaction.

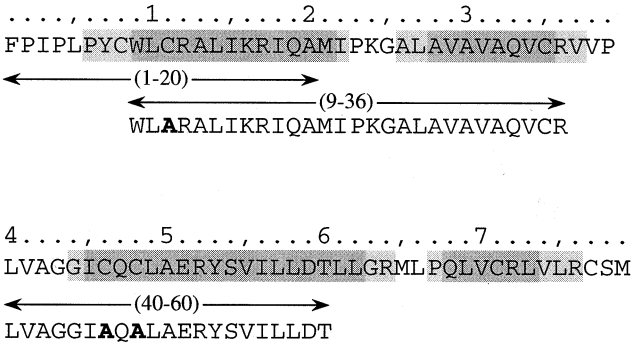

Fig. 1. Sequence of human SP-B and three synthetic peptides. The shading highlights predicted α-helical regions (see text for details); dark gray indicates greater than 70% prediction confidence while light gray indicates a 40–70% confidence level.

2. Material and methods

2.1. Materials

1,2-Dipalmitoyl-*sn*-glycero-3-phosphatidylcholine (DPPC), acyl chain perdeuterated DPPC (DPPC-d_{62}), and 1,2-dipalmitoyl-*sn*-glycero-3-phospho-racemic (1-glycerol) (sodium salt) (DPPG) were obtained from Avanti Polar Lipids (Alabaster, AL) and used without further purification. The reagents and solvents used for peptide synthesis were obtained from Perseptive Biosystems (Framingham, MA). HPLC grade solvents (Aldrich, Milwaukee, WI and Fisher Scientific, Pittsburgh, PA) were used for the purification of peptides and preparation of samples. Hexafluoroisopropanol, *N*-mercaptoacetamide, Trizma hydrochloride (tris(hydroxymethyl)aminomethane hydrochloride), deuterated methanol (CH_3OD), and sodium chloride (99.5%) were obtained from Sigma (St. Louis, MO). Deuterium oxide (^2H_2O, 99.9%) was provided by Cambridge Isotope Laboratories (Andover, MA). HPLC grade H_2O (Fisher Scientific) was used for the water-based subphase. Porcine SP-B was generously provided by Prof. K.M.W. Keough (Memorial University of Newfoundland).

2.2. Peptide design

The sequence of human lung surfactant protein SP-B is shown in Fig. 1. Secondary structure prediction using PredictProgram [26–28] reveals four helical regions. The synthetic peptide fragment SP-B_{1-20} incorporates the first 20 N-terminus amino acids of human SP-B and the first native α-helical region. SP-B_{9-36A} includes the sequence of the first and second α-helical regions and SP-B_{40-60A} includes the sequence of the third native helical region. One Cys residue in SP-B_{9-36A} and two Cys residues in SP-B_{40-60A} were substituted by Ala, as indicated in Fig. 1, to reduce the possibility of forming inter- and/or intramolecular disulfide bonds. Cys to Ala substitution was unnecessary for SP-B_{1-20} since mass spectrometry results showed no indication of cysteine oxidation.

2.3. Peptide synthesis and purification

The peptides were synthesized on a 0.4 mmole scale using a Millipore 9050 Plus peptide synthesizer and standard procedures for solid-phase Fmoc chemistry. The activating technique for the stepwise coupling of amino acids used HATU and the organic base diisopropylethylamine. A PAC-PEG-PS solid support was used to obtain a C-terminal carboxylic acid upon cleavage from the resin. The peptides were deprotected and cleaved with the scavenger cocktail, TFA/phenol/water/triisopropylsilane (88:5:5:2) for 3.5 h. Peptides were then precipitated from the cocktail with cold diethyl ether and filtered to yield crude product.

The SP-B_{1-20} and SP-B_{9-36A} peptides were purified

by reverse-phase HPLC using a Vydac C-4 semi-preparative column. For isolation of SP-B_{1-20}, an eluent gradient of water/acetonitrile, both containing 0.1% TFA, was used. A water/(isopropanol:acetonitrile) (2:1 v/v)-0.1% TFA gradient was employed to purify SP-B_{9-36A}. HPLC was not performed on SP-B_{40-60A} due to the tendency of this peptide to aggregate. The identity and purity of all peptides were confirmed by electrospray mass spectrometry. To eliminate interference from the asymmetric carboxylate stretching band of TFA in the infrared spectrum (approx. 1672 cm^{-1}), the peptides were further treated with 10 mM hydrochloric acid and lyophilized, thus replacing bound TFA counterions with chloride ions.

2.4. Circular dichroism spectroscopy

CD spectra were collected using an AVIV Model 202 Circular Dichroism Spectrometer using a 0.10 cm pathlength cell. Samples were prepared in methanol or ^2H_2O buffer (10 mM Tris HCl, 100 mM NaCl, and 100 μM EGTA, pD 7.2) at approx. 0.20 mg/ml and measurements were done at ambient temperature. The data were fit in a manner that did not rely on peptide concentration.

2.5. Bulk phase FTIR spectroscopy

The FTIR transmission spectra collected for the pure peptides in methanol were obtained at a concentration of approx. 1.5 mg/ml and at ambient temperature. Analysis of the Amide I region was made after subtraction of a pure methanol spectrum from the sample. Multilamellar lipid/peptide vesicles containing either SP-B_{1-20} or SP-B_{9-36A} were prepared by dissolving DPPC and/or DPPG with the appropriate peptide in chloroform/methanol (1:1, v/v). Vesicles containing SP-B_{40-60A} were prepared by dissolving lipid/peptide constituents in chloroform/methanol/hexafluoroisopropanol (1:1:2, v/v/v). The solvents were then evaporated under a slow stream of N_2 gas followed by lyophilization for several hours. Dry samples were rehydrated with ^2H_2O buffer (10 mM Tris HCl, 100 mM NaCl, and 100 μM EGTA, pD 7.2). To promote the formation of multilamellar vesicles and the association of peptide with the bilayer, the samples were repeatedly mixed with vortex action and warmed above the lipid phase transition temperature. Due to the limited supply of peptide, final sample volumes were only approx. 25 μl. Consequently, no attempt was made to separate free and lipid-bound peptide so that multilamellar vesicles in this study may contain a percentage of free peptide. Finally, the pD of the samples was adjusted to 7.2 before insertion between CaF_2 windows enclosing a 25 μm teflon spacer. The temperature of the samples was adjusted using an external circulating water bath (±0.1°C). For analysis of the Amide I region, buffer spectra acquired at the appropriate temperatures were subtracted from sample spectra.

Spectra were obtained using a Mattson RS-1 (Madison, WI) spectrometer with a mercury-cadmium-telluride (MCT) detector. Routinely, 512 interferograms were collected at 4 cm^{-1} spectral resolution, apodized with a triangular function, and Fourier transformed with one level of zero filling to yield spectra encoded at 2 cm^{-1} intervals.

2.6. Monolayer preparation

SP-B_{1-20} and SP-B_{9-36A} were dissolved with and without lipids in chloroform/methanol (2:1, v/v) for both π-A isotherm and IRRAS measurements. Similarly, SP-B_{40-60A} solutions were prepared in chloroform/methanol/hexafluoroisopropanol (1:1:1, v/v/v). Concentrations of samples in organic solution were approx. 1 mg/ml for pure peptide or pure lipid and approx. 1.5 mg/ml for lipid in the binary solutions. ^2H_2O buffer (same as above) was used as the subphase for the IRRAS experiments and an H_2O buffer of the same composition was used for the acquisition of the π-A isotherms.

2.7. π-A isotherms

Isotherms were collected using a temperature controlled NIMA Model 611 trough (maximum surface area 608 cm^2) with a Model PS4 surface pressure sensor (Coventry, UK). The subphase was held at 21±1°C. Typically, 30–40 μl of sample solution was spread at large molecular areas ($\pi = 0$ mN/m) and 45 min were allowed for solvent evaporation

and film relaxation. Monolayers were compressed at approx. 0.04 nm^2/lipid molecule·min for the lipid containing films and approx. 0.15 nm^2/molecule·min for the pure peptide isotherms.

2.8. IRRAS measurements of monolayers

A home-built teflon trough (maximum surface area approx. 90 cm^2) was used and surface pressure of the monolayers was monitored using a Nima (Coventry, UK) Model PS4 surface pressure sensor. Samples containing either pure peptide or peptide mixed with lipid were spread (5–15 μl) onto a clean subphase. This resulted in initial surface pressure values of ≤6 mN/m. The films were allowed to relax for at least 1 h prior to monolayer compression. The subphase temperature was held at 21 ± 1°C for all experiments. Monolayers were intermittently compressed until the desired surface pressure was reached. An additional 0.5 h was permitted for film relaxation before IRRAS spectra were collected. The spectrometer used was a Bio-Rad FTS 40A (Cambridge, MA) equipped with an external MCT detector and home-built optical system. A 35° angle of incidence and unpolarized radiation were used. Interferograms were acquired with the use of a sample shuttle program to compensate for the presence of water vapor rotation-vibration bands in the Amide I region. Details of the experimental setup and data acquisition can be found in Flach et al. [24]. An optical filter (OFC, Natick, MA) was positioned in the path of the incident light to reduce possible heating effects of the IR beam. A total of 1024 scans were acquired at a resolution of 4 cm^{-1}. The scans were co-added and fast-Fourier transformed with one level of zero filling to yield spectra encoded every 2 cm^{-1}.

2.9. Bulk phase IR and IRRAS data analysis

After subtraction, spectra were baseline corrected and smoothed, when necessary, with a second order, seven point Savistky-Golay routine using Grams/32 software (Galactic Industries). IR peak positions were determined using a center of gravity algorithm provided by the National Research Council of Canada.

3. Results

3.1. Bulk phase CD and FTIR spectroscopy of SP-B_{1-20}

CD spectra of SP-B_{1-20} in methanol and ^2H_2O buffer solution are displayed in Fig. 2A and B, respectively. Fitting the CD spectra using the Brahm's basis set [29] reveals predominantly α-helical structure (75 ± 10%) for the peptide in methanol, and approx. 55 ± 10% random coil, 35 ± 10% β-sheet, with up to 10% α-helix for the buffer solution. The IR spectra of the Amide I region for the peptide in methanol and deuterated methanol (CH_3OD) are shown in Fig. 2C. The frequencies observed for the Amide I band in methanol and CH_3OD (1657 and 1651 cm^{-1}, respectively) are indicative of α-helical

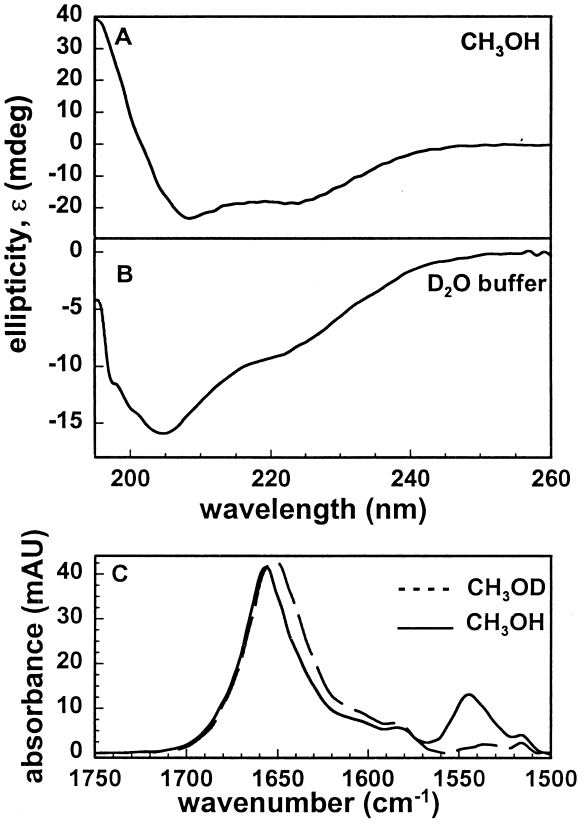

Fig. 2. CD spectra of SP-B_{1-20} in methanol at a concentration of approx. 0.15 mg/ml (A) and in ^2H_2O buffer at a concentration of 0.28 mg/ml (B). (C) IR spectra of the 1750–1500 cm^{-1} region for SP-B_{1-20} in methanol (———) and CH_3OD (- - -) at a concentration of 1.5 mg/ml.

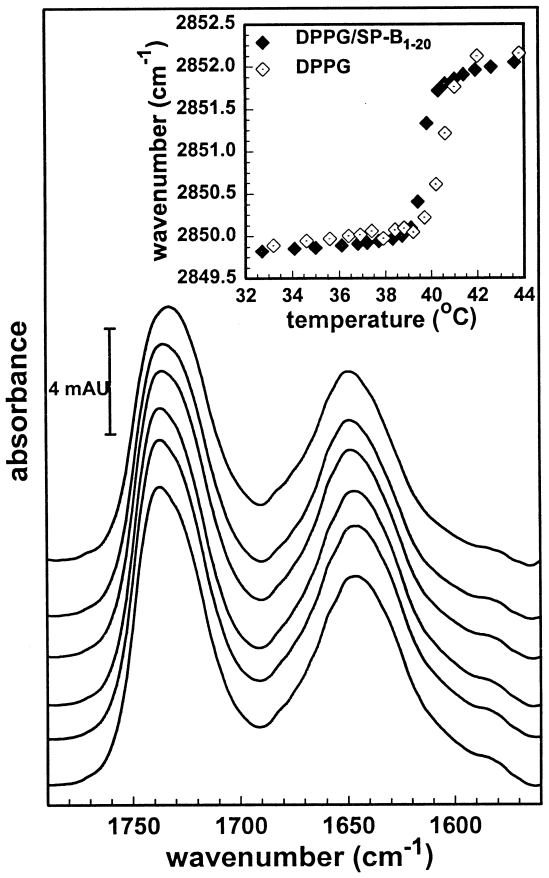

Fig. 3. IR spectra of the 1790–1550 cm^{-1} region for SP-B_{1-20} in multilamellar vesicles of DPPC-d_{62}/DPPG (3:1 lipid mole ratio; 15:1 lipid/peptide mole ratio) in ^2H_2O buffer at temperatures of 26, 30, 33, 37, 42, and 46°C from bottom to top. Inset shows the melting curve (ν_s CH_2) for pure DPPG (◇) and for DPPG/SP-B_{1-20} (◆) multilamellar vesicles over a temperature range of 32–44°C.

structure in both solvents. The 6 cm^{-1} shift to lower frequency in the CH_3OD is due to H→D exchange. The H→D exchange is essentially complete as revealed by the absence of the Amide II band (approx. 1545 cm^{-1}) for the deuterated solvent. The Amide II vibrational mode contains approx. 60% N-H bend. Upon deuteration, the contribution of internal coordinates is altered and the peak is shifted to approx. 1470 cm^{-1} [30].

Fig. 3 displays the 1790–1550 cm^{-1} region of the IR spectra for SP-B_{1-20} with DPPG/DPPC-d_{62} multilamellar vesicles at a 15:1 lipid/peptide molar ratio over a temperature range of 26–46°C. The lipid carbonyl stretching band is observed at approx. 1735 cm^{-1}. The peptide Amide I mode is centered at approx. 1648 cm^{-1}, a frequency typically assigned to H→D exchanged α-helical and/or random coil conformations. The full width at half-height of the Amide I band (approx. 37 cm^{-1}) suggests that various peptide conformers are present which may reflect populations of free and lipid-bound peptide. Similar spectra are observed in the Amide I region for vesicles consisting of either DPPG or DPPC with the peptide. In Fig. 3, small changes are observed in the lipid carbonyl and peptide Amide I band as temperature is increased through the lipid phase transition. The carbonyl band broadens on the low frequency side as the temperature increases, the result of interactions between the C=O group and ^2H_2O. In contrast, the number of the underlying components in the Amide I band and their peak positions, as determined by taking second derivatives of the spectra, did not change with the temperature increase. A slight broadening in the overall Amide I band envelope was noted. IR spectra of SP-B_{1-20} in buffer without lipid (not shown) show a downward shift in the Amide I band (1640 cm^{-1}) indicating an increase in the relative intensity of underlying components typically assigned to random coil and β-sheet structure compared to the peptide with lipid. However, recent studies on solvent-exposed α-helices in aqueous environments report IR Amide I band frequencies as low as 1633 cm^{-1} [31,32]. In addition, quantitative analysis of peptide secondary structure is further complicated by the IR absorption of specific amino acid side chains in the Amide I region [33] which may account for up to approx. 15% of the total Amide I absorption band for the SP-B peptides examined in this study. Therefore, secondary structure assignments herein (Table 1) are performed in a qualitative manner without further data manipulation and take into consideration possible solvent and/or lipid influences on peak position.

The inset in Fig. 3 shows the frequency dependence of the lipid acyl chain symmetric methylene stretching vibration (ν_s CH_2) for DPPG vesicles as a function of temperature in the presence and absence of SP-B_{1-20}. As is evident in the figure, the phase transition temperature of the lipid decreased slightly in the presence of peptide (1–2°C) indicating that the peptide may slightly perturb the lipid acyl chain packing but does not penetrate deeply into the hydrophobic region.

Table 1
IR frequencies and secondary structure of SP-B peptides in various environments

Peptide	Technique	Solvent/subphase	Lipid DPPG	Amide I (cm^{-1})	Secondary structure		
					α-helix	random	β-sheet
$SP\text{-}B_{1-20}$	calculated[a]				60 ± 15[b]		
	CD	CH_3OH	−		75[c]	15	10
	CD	^2H_2O	−		≤10	55	35
	IR	CH_3OH	−	1 657	s[d]		
	IR	CH_3OD	−	1 651	s		
	IR	^2H_2O	−	1 640	m	m	m
	IR	^2H_2O	+	1 648	s	s	w
	IRRAS	^2H_2O	±	1 642	m	m	w
$SP\text{-}B_{9-36A}$	calculated				75 ± 15		
	CD	CH_3OH	−		90	≤10	
	CD	^2H_2O	−		40	50	≤10
	IR	CH_3OH	−	1 657, 1 630	s	w	m
	IR	^2H_2O	+	1 640, 1 627	m	m	s
	IRRAS: low π	^2H_2O	±	1 643	m	m	w
	IRRAS: high π	^2H_2O	±	1 642, 1 624	m	m	s
$SP\text{-}B_{40-60A}$	calculated				75 ± 5		
	IR	^2H_2O	+	1 626	w	w	s
	IRRAS	^2H_2O	±	1 619	w	w	s
porcine SP-B	IRRAS	^2H_2O	−	1 645	m	m	w

[a]Calculated as presented in Fig. 1, see text for details.
[b]Calculated percent helix ± % error.
[c]CD secondary structure predictions ± 10% error.
[d]IR designations are (s) strong, (m) medium, (w) weak.

3.2. π-A isotherms and IRRAS for $SP\text{-}B_{1-20}$

Fig. 4A displays π-A isotherms for DPPG and DPPG/$SP\text{-}B_{1-20}$ monolayers. The isotherm for a pure $SP\text{-}B_{1-20}$ monolayer is shown in the inset. The molecular area for the isotherms obtained from lipid-containing samples is plotted in terms of lipid areas so that the effects due to peptide are easily noted. The increase in molecular area for the isotherm in the presence of peptide compared to the pure lipid isotherm is predominantly due to the surface area occupied by peptide. The liquid expanded/liquid condensed (LE/LC) two phase region observed in the isotherm of pure DPPG as a plateau at π of approx. 10 mN/m does not appear in the presence of the peptide. The kink in the DPPG/$SP\text{-}B_{1-20}$ isotherm at π near 30 mN/m and the merging of the two curves as the limiting area of the lipid is approached are most likely due to loss of the peptide into the subphase. The isotherm of the pure $SP\text{-}B_{1-20}$ peptide (Fig. 4A, inset) shows that the monolayer begins to collapse at a π of approx. 16 mN/m and a limiting area of 0.22 nm^2/residue. The collapse pressure for the pure peptide monolayer is significantly less than the pressure for the binary film at which point peptide loss into the subphase is suspected (approx. 30 mN/m). Considering both the bulk phase lipid melting data (Fig. 3, inset) and the information obtained from the isotherms, both hydrophobic and ionic interactions must be considered between the cationic peptide and anionic lipid. This combined interaction constrains the peptide to the A/W interface over a higher range of pressure for the lipid/peptide mixture compared with the pure peptide monolayer.

The IRRAS spectrum of a pure $SP\text{-}B_{1-20}$ monolayer on ^2H_2O buffer at π of 11 mN/m is shown in Fig. 4B. The frequency of the Amide I band is observed at 1642 cm^{-1} indicative of solvent-exposed α-helical and/or random coil structure. Similar IRRAS spectra were observed over a pressure range of 7–20 mN/m for the pure peptide and for peptide/DPPG monolayers. The relative intensity or integrated area of the lipid carbonyl and peptide Amide I bands can be used to evaluate loss of peptide into

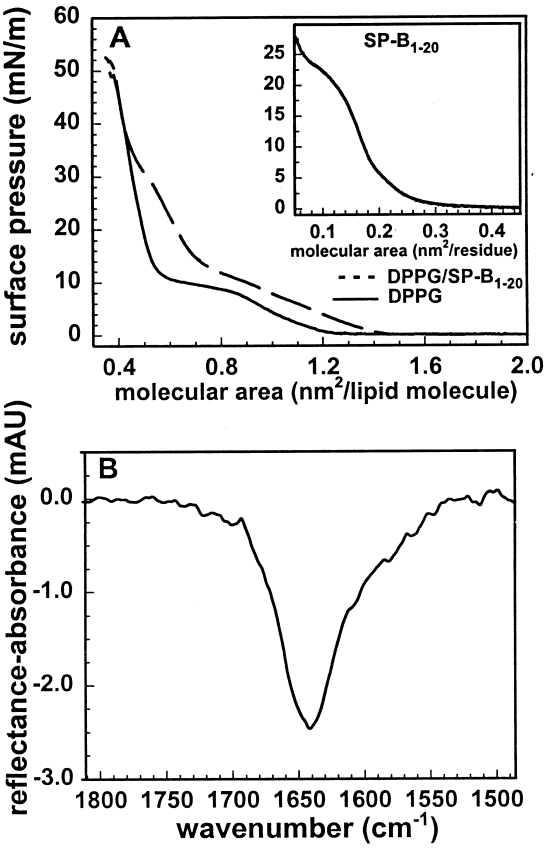

Fig. 4. (A) Surface pressure-molecular area (π-A) isotherms for DPPG (———) and DPPG/SP-B_{1-20} (15:1 mole ratio) (- - -) monolayers. The π-A isotherm of a pure SP-B_{1-20} monolayer is shown in the inset. (B) IRRAS spectrum of the Amide I region for SP-B_{1-20} at a surface pressure of 11 mN/m. Film was spread at an initial surface area of 6 nm^2/molecule yielding an initial surface pressure (π_i) of 2 mN/m. The temperature of the subphase was held at 21 ± 1°C for the H_2O-based buffer used in A and for the ^2H_2O subphase used in B.

the subphase (squeeze out) as a monolayer is compressed [23]. In the current experiment, peptide exclusion is not indicated by relative intensity measurements up to a surface pressure value of 20 mN/m (data not shown). Above a pressure of 20 mN/m, the film is not stable enough to acquire IRRAS spectra which require approx. 15 min/spectrum. When the barrier is stopped at π≥20 mN/m, the rapid drop in surface pressure alone is likely to indicate loss of peptide into the subphase. The surface pressure values at which peptide loss is initiated differs between the π-A isotherm experiments and the IRRAS measurements. This is not surprising, considering the differences in trough size and compression method. Slight broadening on the low frequency side of the Amide I band in the IRRAS spectrum (Fig. 4B) indicates a small degree of β-sheet structure or surface aggregation. The similarity between the Amide I band position and bandwidth for the pure peptide in bulk and monolayer phases suggests that the structure is approximately the same in both environments. An Amide I band was not observed for DPPC/SP-B_{1-20} monolayers at either 15:1 and 15:2 molar ratios. The absence of an Amide I band implies that the cationic peptide dissolves in the subphase and is not associated with the zwitterionic lipid monolayer. This in turn suggests that the hydrophobic interaction between the lipid acyl chains and peptide at the air/water interface is indeed weak.

3.3. *Bulk phase CD and FTIR spectroscopy of SP-B_{9-36A}*

Fig. 5A and B display CD spectra for SP-B_{9-36A}

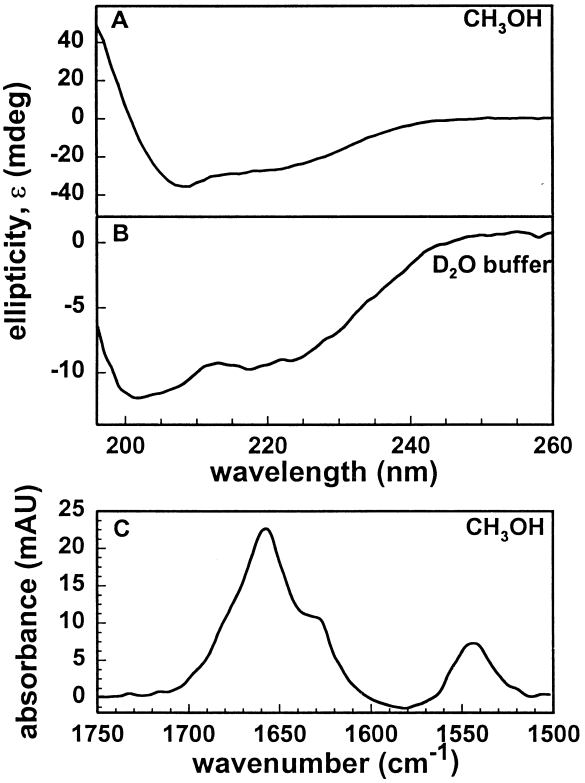

Fig. 5. CD spectra of SP-B_{9-36A} in methanol (A) and ^2H_2O buffer (B) at a concentration of approx. 0.15 mg/ml. (C) IR spectrum of the 1750–1500 cm^{-1} region for SP-B_{9-36A} in methanol at a concentration of 1.5 mg/ml.

dissolved in methanol and ^2H_2O buffer, respectively. Fitting of the CD data with the Brahm's basis set reveals approx. 90 ± 10% α-helical structure for the peptide in methanol and 50 ± 10% random coil, 40 ± 10% α-helix, with up to 10% β-sheet structure in buffer. In Fig. 5C, two major components are observed in the IR spectrum of the Amide I region at 1657 and 1630 cm^{-1} for SP-B_{9-36A} dissolved in methanol. The former is indicative of α-helical structure and the latter of antiparallel β-sheet. The less intense, high frequency component of antiparallel β-sheet structure is barely discernable as a small shoulder at approx. 1695 cm^{-1}. The concentration of peptide required for transmission IR is an order of magnitude greater than that used for CD spectroscopy (1.5 mg/ml versus 0.15 mg/ml, respectively). It is likely that the higher concentration induces the formation of intermolecular β-sheet for the peptide dissolved in methanol. SP-B_{9-36A} was not sufficiently soluble in buffer to obtain an IR spectrum with an acceptable signal to noise level.

Bulk phase IR spectra for DPPG/SP-B_{9-36A} (15:1, molar ratio) multilamellar vesicles at various temperatures are shown in Fig. 6. Since the 9-36A peptide is not readily soluble in buffer and contains a region of hydrophobic amino acids near its C-terminal, the peptide is likely bound to the vesicles in this preparation. The inset in Fig. 6 displays ν_s CH_2 as a function of temperature for DPPG in the presence and absence of the peptide. The phase transition of the lipid is unaffected by the presence of SP-B_{9-36A}. As the lipid acyl chains melt, the C = O stretching band (approx. 1735 cm^{-1}) broadens on the low frequency side indicating hydration of the ester carbonyl. The breadth of the peptide Amide I band envelope is due to the presence of several underlying components. The two primary bands in the envelope are located at 1627 and 1640 cm^{-1}, indicative of β-sheet and solvated α-helical/random coil structure, respectively. A greater proportion of β-sheet structure is observed in the IR compared to the CD spectra for the peptide in buffer, consistent with the concentration-dependent formation of intermolecular β-sheet as found for the peptide dissolved in methanol. A slight broadening on the high frequency side of the Amide I band is observed (Fig. 6) as temperature increases.

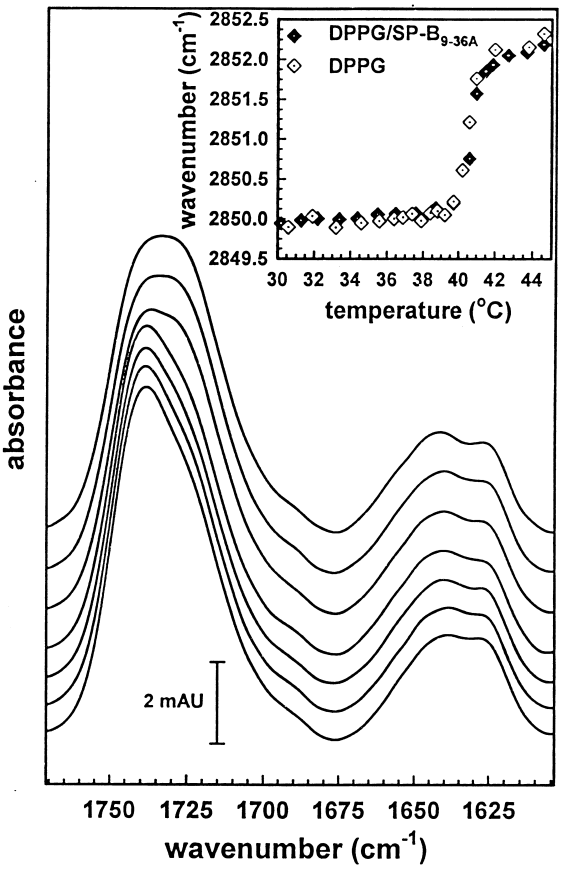

Fig. 6. IR spectra of the 1775–1605 cm^{-1} region for DPPG/SP-B_{9-36A} multilamellar vesicles (15:1 mole ratio) at temperatures of 26, 31, 37, 40, 41, 46, and 50°C from bottom to top. Inset shows the melting curve (ν_s CH_2) for pure DPPG (◇) and for DPPG/SP-B_{9-36A} (◆) over a temperature range of 30–46°C.

3.4. π-A isotherms and IRRAS for SP-B_{9-36A}

Fig. 7A displays π-A isotherms for pure DPPG and DPPG/SP-B_{9-36A} monolayers. The isotherm for a pure SP-B_{9-36A} monolayer is shown in the inset. An increase in molecular area is observed for the entire DPPG/SP-B_{9-36A} isotherm compared to the isotherm for pure DPPG. This is predominantly due to surface area occupied by peptide. The LE/LC two phase coexistence region ($\pi \approx 10$ mN/m) observed in the pure lipid film is essentially abolished in the binary film. An inflection point is noted for the binary film at a surface pressure of 36 mN/m which is most likely due to some loss of peptide from the surface. As pressure is increased, however, the two curves do not merge to the limiting area of the lipid,

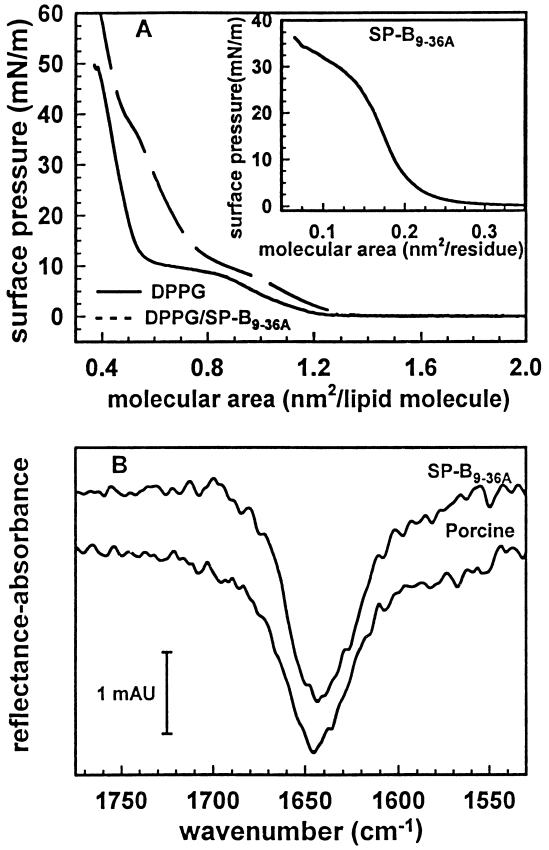

Fig. 7. (A) Surface pressure-molecular area (π-A) isotherms of DPPG (———) and DPPG/SP-B_{9-36A} (15:1 mole ratio) (- - -) at the air/water interface. π-A isotherm of SP-B_{9-36A} is shown in the inset. (B) IRRAS spectra of the Amide I region for SP-B_{9-36A} and for porcine SP-B at $\pi \approx 15$ mN/m. The temperature of the ^2H_2O buffer subphase was held at 21 ± 1°C. Upon spreading, the initial area for SP-B_{9-36A} was 7.7 nm^2/molecule yielding $\pi_i = 4$ mN/m and for porcine SP-B, the area was 28 nm^2/molecule with $\pi_i = 6$ mN/m.

in contrast to SP-B_{1-20}. This suggests that a percentage of SP-B_{9-36A} remains at the surface at high pressure. For the pure peptide (inset), film collapse begins at π of approx. 24 mN/m and at a limiting area of 0.22 nm^2/residue. The collapse pressure for SP-B_{9-36A} is significantly higher than that observed for SP-B_{1-20} ($\pi \approx 16$ mN/m), whereas the limiting area (0.22 nm^2/residue) is the same for both. In addition, the isotherm observed for SP-B_{9-36A} is more condensed than for SP-B_{1-20}. The combination of a higher collapse pressure and a more condensed isotherm indicate that intermolecular interactions provide a greater degree of stabilization for the SP-B_{9-36A} monolayer compared to SP-B_{1-20}.

IRRAS spectra of the Amide I region for porcine SP-B and SP-B_{9-36A} at $\pi = 15$ mN/m are displayed in Fig. 7B. The position (approx. 1644 cm^{-1}) of the Amide I bands are similar for both monolayers at $\pi \leq 15$ mN/m and are indicative of random coil or mixed helix/random coil structure. The bandwidth for SP-B_{9-36A} is slightly broadened on the low frequency side compared to porcine SP-B. However as the pressure is increased to 30 mN/m, the Amide I band of SP-B_{9-36A} displays a noteworthy change while the band for the native SP-B remains essen-

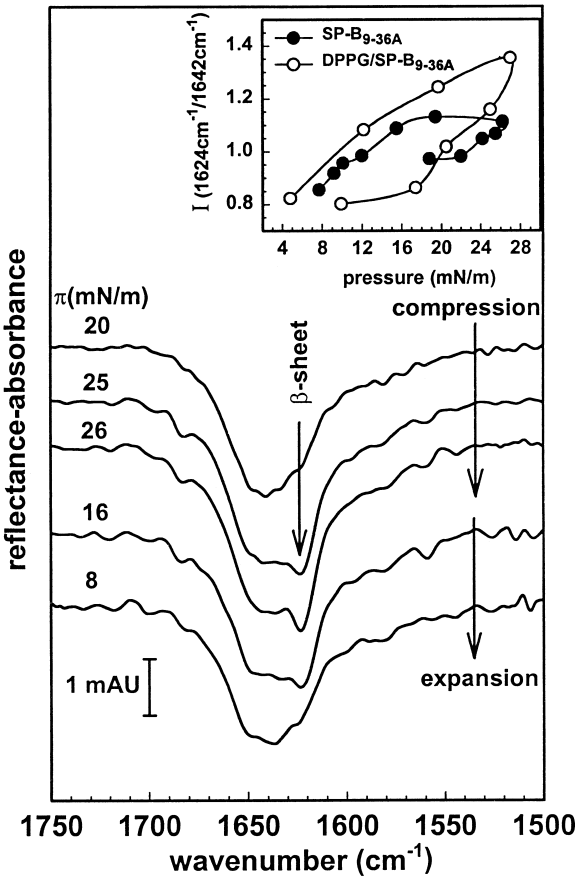

Fig. 8. IRRAS spectra of the 1750–1500 cm^{-1} region for SP-B_{9-36A} at the air/^2H_2O interface at various surface pressure values. The film was spread using the same initial conditions as in Fig. 7B. Spectra are plotted from top to bottom at specified π values during monolayer compression and subsequent expansion. A minimum equilibration time of 1 h was permitted between monolayer expansion and IRRAS data acquisition. The inset displays the intensity (I) dependence of underlying Amide I band components as a function of surface pressure for compression and expansion in the presence (○) and absence (●) of DPPG. The subphase temperature was held at 21 ± 1°C.

tially the same (data not shown for pressure dependence of porcine SP-B). Fig. 8 displays IRRAS spectra of the Amide I region for a SP-B_{9-36A} monolayer at various surface pressure values during compression and subsequent expansion. Most interesting is the reversible surface pressure-induced formation of β-sheet structure. As the monolayer is compressed to $\pi > 20$ mN/m, the Amide I component attributed to β-sheet structure at 1624 cm^{-1} becomes prominent. Subsequently, as the surface area available to the film is increased (film expansion) and π decreases, the intensity of the Amide I component at 1624 cm^{-1} decreases. The pressure dependence of the Amide I profile is shown in the inset of Fig. 8 as the intensity ratio of the Amide I band components at 1624/1642 cm^{-1} versus surface pressure. Results are shown for both pure SP-B_{9-36A} peptide and DPPG/SP-B_{9-36A} monolayers. Similar behavior is observed in the presence and absence of the lipid when the initial surface pressure (π_i, π before compression begins) is ≤4 mN/m. When monolayers were spread so that the initial surface pressure (π_i) was 16 mN/m (condensed phase), β-sheet formation was not induced by an increase in pressure (data not shown). Apparently, a large molecular area is initially required for reversible β-sheet formation to take place. The extent of peptide exclusion from the surface cannot be evaluated for SP-B_{9-36A} due to changes in its secondary structure with compression. Extinction coefficients for various secondary structures have not been reported for monolayers precluding a quantitative analysis of peptide loss.

3.5. *Bulk phase and monolayer FTIR spectroscopy for SP-B_{40-60A}*

The SP-B_{40-60A} peptide has a tendency to aggregate; therefore, only a limited number of experiments were accessible. The bulk phase IR spectrum of the 1800–1575 cm^{-1} region for DPPG/SP-B_{40-60A} multilamellar vesicles is shown in Fig. 9A. The main component of the Amide I band is found at 1626 cm^{-1} for the lipid/peptide sample at a 15:1 mole ratio and remains unchanged as the amount of lipid is increased to 50:1 (data not shown). An Amide I frequency of 1626 cm^{-1} along with the presence of a weak component at approx. 1685 cm^{-1} is consistent with antiparallel β-sheet structure. A small shoulder is observed at approx. 1650 cm^{-1} which may be due to the presence of a minor helical or random coil component. The small contribution observed at approx. 1673 cm^{-1} may be due to residual TFA. In addition, the Amide I band for micelles consisting of lyso-PC and SP-B_{40-60A} in a 15:1 molar ratio is also observed at 1626 cm^{-1}.

An IRRAS spectrum of the 1800–1540 cm^{-1} region for DPPG/SP-B_{40-60A} is presented in Fig. 9B with the Amide I region for the pure peptide monolayer shown in the inset. The major component of the Amide I band for both the single and binary monolayers is observed at approx. 1619 cm^{-1}. Amide I bands observed at lower frequencies (< 1620 cm^{-1}) have been attributed to the formation of intermolec-

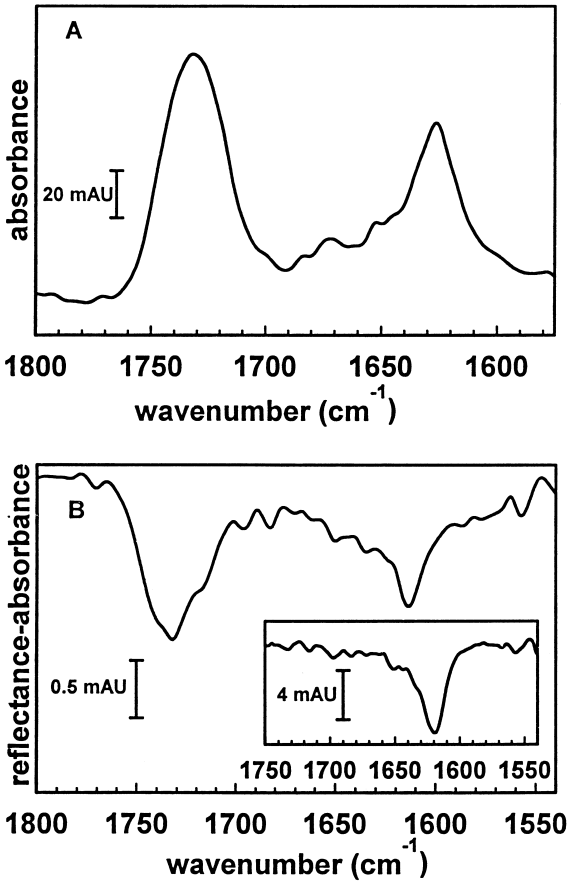

Fig. 9. (A) IR spectrum of the lipid carbonyl and the peptide Amide I region for DPPG/SP-B_{40-60A} multilamellar vesicles in ^2H_2O buffer at a molar ratio of 15:1 and temperature of 15°C. (B) IRRAS spectra of SP-B_{40-60A} (inset) and DPPG/SP-B_{40-60A} monolayers (15:1 mole ratio) at surface pressures of 14 and 21 mN/m, respectively. $\pi_i \approx 0$ mN/m for both monolayers and the temperature of the ^2H_2O buffer subphase was 21 ± 1°C.

ular β-sheet aggregates where the low frequency suggests the presence of strong hydrogen bonds [34]. Similar to the bulk phase IR spectrum, a small shoulder is observed on the high frequency side of the Amide I band. The relative intensity of these components remains the same upon compression and expansion of either the pure peptide or binary monolayers.

4. Discussion

Several reports evaluating the secondary structure and surface activity of peptides with sequences based on the lung surfactant protein SP-B have recently appeared with correlations drawn between structure and function. In addition to providing insight into the minimal requirements needed to mimic the putative in vivo function of SP-B, the peptides are primarily being evaluated for potential therapeutic applications. In the majority of the studies, the secondary structure and lipid interactions of the peptides are determined by IR or CD spectroscopy in bulk phase systems such as organic solution, SDS micelles, and lipid vesicles [18,19,35,36]. However, the secondary structure and orientation of peptides and proteins may differ between bulk and monolayer environments due to the different forces at work [20,37–40]. Since it is thought that one of the major functions of SP-B is to enhance the adsorption of surfactant to the air/alveolar lining, it becomes essential to evaluate molecular structure in an environment that mimics this interface. Relatively few techniques can provide molecular conformation and orientation at the air/water interface. In the current investigation, IRRAS, has been applied to provide protein and peptide structural information at the air/water interface. Concurrently, experimental parameters that are thought to be relevant to surfactant function and easily controlled using a Langmuir trough such as surface pressure and therefore molecular density, are not readily controlled under bulk phase conditions and are shown here to provide pertinent information about peptide structure in lipid films. A comparison of protein secondary structure in bulk and monolayer environments may provide a more complete picture of the role surfactant proteins play in respiration. The following discussion will review the conformation of each of the three peptides and their interaction with lipids in various environments (see Table 1) and compare these results with previous reports. The advantages and disadvantages of the applied techniques will also be addressed.

The secondary structure of SP-B_{1-20} is strongly dependent on solvent/environment. In the structure promoting solvent, methanol, the peptide is predominantly α-helical whereas a mixed motif is observed in buffer from both CD (Fig. 2) and IR spectra. In addition, the presence of lipid in the bulk phase appears to prevent or limit the formation of β-sheet, and a mixed helical/random coil structure is detected (Fig. 3). Reports on a similar peptide, composed of the first 25 residues of native SP-B (SP-B_{1-25}), are comparable with the results for SP-B_{1-20}. A dominant α-helical content with minor contributions from β-turn and disordered segments was reported based on CD and IR spectra of the 1-25 peptide in structure-promoting environments such as methanol, TFE, SDS micelles, and lipid films [36].

Although the approach is widely applied, it is difficult to predict peptide conformation at the A/W interface based on limiting areas determined from π-A isotherms. Limiting areas are affected by the orientation of ordered segments and the analysis may further be complicated by the presence of more than one secondary structure. Limiting areas are assumed to be determined prior to the development of loops or tails projecting above or below the surface [41]. The limiting area of 0.22 nm^2/residue observed in the π-A isotherm for SP-B_{1-20} is in the range reported for β-sheet or random coil peptides lying in the interface [42,43]. The IRRAS Amide I band spectral parameters indicate that a mixture of secondary structures are present with dominant solvent-exposed α-helical/random coil components and a small amount of β-sheet or aggregated structure. The Amide I band profiles observed for pure peptide and lipid/peptide monolayers are very similar to each other unlike the bulk phase system where the presence of lipid appears to limit β-sheet formation or aggregation. Bulk phase lipid melting curves for DPPG indicate that in the presence of peptide a slight disturbance of lipid acyl chain packing occurs (Fig. 3, inset), consistent with the increase in molecular area shown in the isotherms (Fig. 4). In addition, the merging of the two isotherms at high pres-

sure indicates that this hydrophobic interaction is not a strong one and subsequent monolayer experiments comparing the interaction of SP-B_{1-20} with DPPC versus DPPG indicate that ionic forces play the predominant role at the air/water interface. In either case (both bulk phase and monolayer), the results indicate that the peptide does not deeply insert into the lipid acyl chain region and are consistent with previous ESR and fluorescence investigations of SP-B_{1-25} with lipids which demonstrate that the bulk of the peptide resides near the lipid polar head group region with slight perturbation to the acyl chains [36].

Bulk phase IR and IRRAS spectra of the SP-B_{40-60A} peptide are indicative of predominantly antiparallel β-sheet and β-sheet/aggregated structures, respectively. Perturbations to lipid acyl chain melting transitions and π-A isotherms due to the presence of the 40-60 peptide could not be evaluated because of residual hexafluoroisopropanol which was necessary to dissolve the peptide and could not be removed from the lipid phase. An earlier fluorescence study on SP-B analogues reported that the 40-60 peptide significantly perturbed the interior of DPPC/DPPG lipid bilayers [44].

The most striking behavior is displayed by SP-B_{9-36A} monolayers where reversible surface pressure-induced β-sheet formation is observed. Although bulk phase IR spectra of the 9-36 peptide with lipid show contributions from α-helical, random coil, and β-sheet structure, changes in relative amounts of these components analogous to those observed in monolayers does not occur. It is also important to note that the π-A isotherms for the peptide-containing monolayers (Fig. 7) do not display a distinctive kink or similar feature that would indicate a change in secondary structure has been initiated. Therefore, it is evident that surface pressure-based methods for secondary structure determination of SP-B_{9-36A} in aqueous monolayers may lead to erroneous conclusions. The observation that SP-B_{9-36A} is retained in the binary monolayers at higher pressures (Fig. 7A) may have implications for the native protein's surface active properties. It seems reasonable to suggest that the sequence of this peptide contains one of the domains in native SP-B that is responsible for promoting adsorption and spreading of lipids.

Taken together, the current observations reveal the presence of subtle forces at work to produce the secondary structure of native SP-B. The intact protein possesses negligible β-sheet content in monolayers [23] with varying, small amounts reported in the bulk phase [7–9]. All three synthetic peptides reveal the presence of this secondary structure, but the context in which the structure forms is different for each peptide. SP-B_{40-60A} simply aggregates in aqueous media via the formation of extended β-like forms. The aggregation is most likely inhibited in the intact protein. SP-B_{1-20} displays a β-sheet structure in aqueous environments but not in helix-promoting or lipidic environments. Evidently, the tertiary structure of native SP-B (perhaps in lipidic environments) sequesters this fragment from purely aqueous contacts. Most interesting is the reversible surface pressure induced formation of β-sheet structures in SP-B_{9-36A} monolayers at the A/W interface. No comparable experiment can be performed in bulk phases. Presumably, the β-sheet forms in this instance to decrease the surface area occupied by the peptide in response to the increased pressure. Thus the three fragments in this study are each in some sense 'poised' to form β-sheet structures. The formation of these structures is precluded by the tertiary structure/environment of the intact protein under normal conditions; however, it is possible that under extreme conditions (as are found at the air/alveolar lining) secondary structure modulation can occur.

The advantages of IRRAS are substantial for the study of peptide secondary structure in monolayers. First, other spectroscopic methods are simply not applicable. Second, the use of π-A isotherms (the only other technology widely applied to this problem) to determine secondary structures is flawed. Finally, there is a long history of IR spectra-structure correlations that provide a basis for data interpretation.

In view of the conformational heterogeneity (in particular the presence of random coil and aggregated structure) observed for the peptides at the air/water interface, our initial goal of determining orientation will have to depend on isotopic labeling experiments to permit the examination of specific, ordered regions within the peptides. In addition, investigations aimed at evaluating the conformational

behavior of SP-B_{9-36A} in morphologically relevant environments are underway.

Acknowledgements

This work was supported by US Public Health Service grant GM 29864 to RM.

References

[1] J. Goerke, Biochim. Biophys. Acta 1408 (1998) 79–89.
[2] J. Johansson, T. Curstedt, Eur. J. Biochem. 244 (1997) 675–693.
[3] L. Creuwels, L.M.G. van Golde, H.P. Haagsman, Lung 175 (1997) 1–39.
[4] F.J. Walther, J. Hernández-Juviel, R. Bruni, A.J. Waring, Am. J. Respir. Crit. Care Med. 156 (1997) 855–861.
[5] J. Johansson, M. Gustafsson, M. Palmblad, S. Zaltash, B. Robertson, T. Curstedt, Biodrugs 11 (1999) 71–77.
[6] S. Hawgood, M. Derrick, F. Poulain, Biochim. Biophys. Acta 1408 (1998) 150–160.
[7] G. Vandenbussche, A. Clercx, T. Curstedt, J. Johansson, H. Jörnvall, J.M. Ruysschaert, Eur. J. Biochem. 203 (1992) 201–209.
[8] J. Pérez-Gil, A. Cruz, C. Casals, Biochim. Biophys. Acta (1993) 261–270.
[9] M.R. Morrow, J. Pérez-Gil, C. Boland, G. Simatos, J. Stewart, D. Absolom, V. Sarin, K.M.W. Keough, Biochemistry 32 (1993) 4397–4402.
[10] A. Cruz, C. Casals, J. Pérez-Gil, Biochim. Biophys. Acta 1255 (1995) 68–76.
[11] J.E. Baatz, B. Elledge, J.A. Whitsett, Biochemistry 29 (1990) 6714–6720.
[12] A. Cruz, C. Casals, I. Plasencia, D. Marsh, J. Pérez-Gil, Biochemistry 37 (1998) 9488–9496.
[13] K. Shiffer, S. Hawgood, H.P. Haagsman, B. Benson, J.A. Clements, J. Goerke, Biochemistry 32 (1993) 590–597.
[14] J.D. Vincent, S.D. Revak, C.G. Cochrane, I.W. Levin, Biochemistry 30 (1991) 8395–8401.
[15] A.S. Dico, J. Hancock, M.R. Morrow, J. Stewart, S. Harris, K.M.W. Keough, Biochemistry 36 (1997) 4172–4177.
[16] A. Cruz, D. Marsh, J. Pérez-Gil, Biochim. Biophys. Acta 1415 (1998) 125–134.
[17] A. Cruz, C. Casals, K.M.W. Keough, J. Pérez-Gil, Biochem. J. 327 (1997) 133–138.
[18] J.H. Kang, M.K. Lee, K.L. Kim, K.-S. Hahm, Biochem. Mol. Biol. Int. 40 (1996) 617–627.
[19] A.J. Waring, K.F. Faull, C. Leung, A. Chang-Chien, P. Mercado, H.W. Taeusch, L.M. Gordon, Pept. Res. 9 (1996) 28–39.
[20] D. Dieudonné, A. Gericke, C.R. Flach, X. Jiang, R.S. Farid, R. Mendelsohn, J. Am. Chem. Soc. 120 (1998) 792–799.
[21] M.A. Oosterlaken-Dijksterhuis, H.P. Haagsman, L.M.G. van Golde, R.A. Demel, Biochemistry 30 (1991) 10965–10971.
[22] C.R. Flach, J.W. Brauner, J.W. Taylor, R.C. Baldwin, R. Mendelsohn, Biophys. J. 67 (1994) 402–410.
[23] B. Pastrana-Rios, S. Taneva, K.M.W. Keough, A.J. Mautone, R. Mendelsohn, Biophys. J. 69 (1995) 2531–2540.
[24] C.R. Flach, A. Gericke, R. Mendelsohn, J. Phys. Chem. 101 (1997) 58–65.
[25] A. Gericke, C.R. Flach, R. Mendelsohn, Biophys. J. 73 (1997) 492–499.
[26] B. Rost, C. Sander, Proc. Natl. Acad. Sci. USA 90 (1993) 7558–7562.
[27] B. Rost, C. Sander, J. Mol. Biol. 232 (1993) 584–599.
[28] B. Rost, C. Sander, Proteins 19 (1994) 55–72.
[29] N.J. Greenfield, Anal. Biochem. 235 (1996) 1–10.
[30] T. Miyazawa, Y. Shimanouchi, S. Mizushima, J. Chem. Phys. 29 (1958) 611–616.
[31] R. Gilmanshin, S. Williams, R.H. Callender, W.H. Woodruff, R.B. Dyer, Proc. Natl. Acad. Sci. USA 94 (1997) 3709–3713.
[32] S. Williams, T.P. Causgrove, R. Gilmanshin, K.S. Fang, R.H. Callender, W.H. Woodruff, R.B. Dyer, Biochemistry 35 (1996) 691–697.
[33] S.Y. Venyaminov, N.N. Kalnin, Biopolymers 30 (1990) 1243–1257.
[34] I.H.M. van Stokkum, H. Linsdell, J.M. Hadden, P.I. Haris, D. Chapman, M. Bloemendal, Biochemistry 34 (1995) 10508–10518.
[35] R. Bruni, W.H. Taeusch, A.J. Waring, Proc. Natl. Acad. Sci. USA 88 (1991) 1–6.
[36] L.M. Gordon, S. Horvath, M.L. Longo, J.A.N. Zasadzinski, H.W. Taeusch, K. Faull, C. Leung, A.J. Waring, Protein Sci. 5 (1996) 1662–1675.
[37] H. Chen, S.L. Hsu, D.A. Tirrell, Langmuir 13 (1997) 4775–4778.
[38] I. Cornut, B. Desbat, J.M. Turlet, J. Dufourcq, Biophys. J. 70 (1996) 305–312.
[39] M. Boncheva, H. Vogel, Biophys. J. 73 (1997) 1056–1072.
[40] F. Wu, C.R. Flach, B.A. Seaton, T.R. Mealy, R. Mendelsohn, Biochemistry 38 (1999) 792–799.
[41] F. MacRitchie, Chemistry at Interfaces, Academic Press, San Diego, CA, 1989.
[42] W.F. DeGrado, J.D. Lear, J. Am. Chem. Soc. 107 (1985) 7684–7689.
[43] K.E. Krebs, J.A. Idbah, M.C. Phillips, Biochim. Biophys. Acta 959 (1988) 229–237.
[44] J.E. Baatz, V. Sarin, D.R. Absolom, C. Baxter, J.A. Whitsett, Chem. Phys. Lipids 60 (1991) 163–178.